ACS NANOSCIENCE Au
AN OPEN ACCESS JOURNAL OF THE AMERICAN CHEMICAL SOCIETY

pubs.acs.org/nanoau
Article

Metabolomics Analysis for Unveiling the Toxicological Mechanism of Silver Nanoparticles Using an *In Vitro* Gastrointestinal Digestion Model

Yongjiu Chen, Ruixia Wang,* and Ming Xu

Cite This: *ACS Nanosci. Au* 2024, 4, 327−337
Read Online

ABSTRACT: The increasing use of silver nanoparticles (AgNPs) in consumer products has led to concerns about potential health risks after oral exposure as a result of the transformation and absorption in the gastrointestinal tract (GIT). However, the intricate condition of the GIT poses challenges in understanding the fate and toxicity of AgNPs as they traverse from the mouth to the rectum. For an in-depth understanding of the nanobio interactions, we employed a simulated digestion model to investigate alterations in the physicochemical properties of AgNPs *in vitro*. Meanwhile, we investigated the underlying toxicological mechanisms of digested AgNPs in enterocytes through metabolomics analysis. In contrast to route means that primarily apply salt solutions to mimic dietary digestion, this *in vitro* model is a semidynamic sequential digestion system that includes artificial oral, gastric, and intestinal fluids, which are similar to those under physiological conditions including electrolytes, enzymes, bile, pH, and time of digestion. Our results suggest that the formation of Ag−Cl and Ag−S species within the simulated digestion model can lead to an increase in the size of digested AgNPs and that the acidic condition promotes the release of Ag^+ from particles. More critically, the presence of digestive enzymes and high concentrations of salt enhances the uptake of Ag by human colon enterocytes, ultimately promoting ROS generation and exacerbating cytotoxicity. Metabolomics analysis further reveals that the sequentially digested AgNPs may disorder lipid metabolism, including the biosynthesis of unsaturated fatty acids and arachidonic acid metabolism, thus increasing the possibility of ferroptosis activation in enterocytes. These findings offer significant insights into the fate and potential adverse effects of AgNPs in the GIT, providing important implications for assessing the health risks of AgNPs via oral exposure.

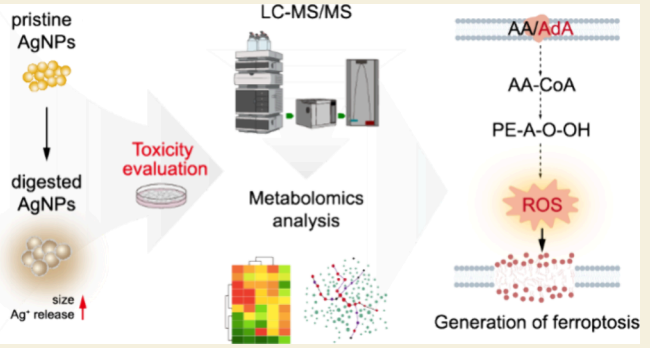

KEYWORDS: *silver nanoparticles, oral exposure, gastrointestinal tract, cytotoxicity, toxicological mechanism*

INTRODUCTION

Silver nanoparticles (AgNPs) have been widely utilized in consumer products and medical applications because of their excellent broad-spectrum antibacterial, antiviral, and antifungal properties.[1] For example, AgNPs have been applied as food additives or inner coating for various food storage containers, such as plastic bags or boxes, to prolong the shelf life of food.[2,3] It is estimated that the usage of AgNPs in food products can lead to an uptake of Ag up to 0.02 mg kg^{-1} body weight per day.[4] In particular, some Ag-containing products, such as plush toys, breast milk storage bags, and sippy cups, may bring potential risks to children.[5] For instance, Mackevica et al. found that breast milk pack contained approximately 31.2 mg Ag/kg.[6] Quadros et al. determined a release of 0.93−24.3 mg Ag/kg from sippy cup products to juice.[5] Therefore, oral ingestion is considered as a primary way of exposure to AgNPs for the public.

Numerous animal studies have demonstrated that AgNPs could be found in the intestine after being orally ingested,[7−11] and the chronic oral exposure to AgNPs damaged the epithelial cell microvilli and increased numbers of goblet cells in the intestine, suggesting that AgNPs may disorder the intestinal immune microenvironment.[12−15] The accumulation of AgNPs in the intestine can causes inflammation, through damaging the epithelial barrier and activating immune cells. This leads to their infiltration in the intestinal lining, the activation of transcription factors like nuclear factor kappa B (NF-κB), and the release of inflammatory substances such as cytokines and chemokines.[16,17] Recent studies reported that the oral exposure of AgNPs can also induce disturbances in the gut

Received: April 15, 2024
Revised: June 5, 2024
Accepted: June 7, 2024
Published: June 25, 2024

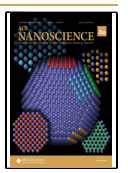

microbiota.[18,19] Ultimately, these events will contribute to the development or worsening of various gut diseases, such as inflammatory bowel diseases (IBDs, such as Crohn's disease and ulcerative colitis).[20−22] Although the toxic effects of AgNPs in the gastrointestinal tract (GIT) have been confirmed, the gastrointestinal fate of AgNPs, including transformation and subsequent cellular interactions, remains not well understood, which is of key importance to assess their health risks.[23−25] Consequently, an *in vitro* digestive simulation is necessary to specifically explore the correlation between the transformation and toxicity of AgNPs during gastrointestinal digestion.

Many studies focused on using salt solutions as gastrointestinal simulants to explore the transformation of AgNPs in the GIT. For example, Mwilu et al. applied a synthetic human stomach fluid for exploring the transformation of AgNPs, showing that digested AgNPs tended to aggregate and release Ag^+, potentially affecting the toxicity of AgNPs.[26] Abdelkhaliq et al. revealed that *in vitro* digested AgNPs influenced their dissolution properties and uptake/association with the Caco-2/HT29-MTX monolayer.[27] However, there are still many knowledge gaps regarding the behaviors of AgNPs differing in salt solutions, digestive enzymes, and bile salts upon their toxic effects toward enterocytes, and the underlying toxicological mechanisms. Recently, an *in vitro* digestion model has been developed and recommended by the international INFOGEST network composed of multidisciplinary experts from over 35 countries.[28] This model employs a semidynamic simulation approach to mimic the digestive processes of the human GIT using constant ratios of substrates to enzymes and electrolytes, as well as constant pH values for each digestion phase. By adhering to experimental conditions based on physiological data, this method approximates *in vitro* equivalents effectively, making it well-suited for mechanistic studies. On the other side, metabolomics has been widely used as a toxicological approach enabling comprehensive profiling of metabolites within cells and tissues in response to stressors.[29] But, there is only one study focusing on the effect of digested AgNPs on fecal fermentation using an *in vitro* digestion model with untargeted metabolomics analysis.[30] Therefore, understanding the metabolic perturbations induced by sequentially digested AgNPs in the GIT can provide more insights into their toxicological mechanisms.

In this study, to explore the transformation and toxic effects of AgNPs in conditions close to the real GIT, we first developed an *in vitro* digestion model with simulated digestive fluids based on a standard protocol to characterize the transformation of AgNPs in the presence or absence of digestive enzymes. Afterwards, we investigated the cytotoxicity of sequentially digested AgNPs in enterocytes and the potential toxicological mechanisms through metabolomics analysis. By integrating chemical and biological changes, we aim to unveil the fate and cytotoxicity of AgNPs in the GIT.

2. EXPERIMENTAL SECTION

2.1. Synthesis of AgNPs

Citrate-capped AgNPs were synthesized via a chemical reduction method using sodium borohydride ($NaBH_4$) as a reducing agent and trisodium citrate as a stabilizing agent, as previously reported.[31] In detail, 75 mL trisodium citrate solution (1% (w/v), 99.5%, Beijing Solarbio Science & Technology, China, No. S8220) was heated to 70 °C and then mixed with 1.7 mL $AgNO_3$ solution (1% (w/v), Sinopharm Chemical Reagent, China, No. CFSR-10018464) followed by rapid addition of 2 mL freshly prepared $NaBH_4$ solution (0.1% (w/v), 98%, Sinopharm Chemical Reagent, China, No. 80115865). The mixture was stirred for 1 h at 70 °C and then cooled to room temperature with continuous stirring and addition of deionized H_2O to reach a volume of 100 mL to obtain the seed solution. Subsequently, 2 mL of 1% (w/v) trisodium citrate solution was added into 80 mL of deionized H_2O and boiled for 15 min. The resulting solution was vigorously stirred and mixed with 10.0 mL of seed solution and 1.7 mL of 1% (w/v) $AgNO_3$ solution. The mixture was stirred for an additional hour under reflux conditions and then cooled to room temperature. After being centrifuged using ultrafiltration centrifugal tubes (Sartorius, MWCO: 30 kDa, Germany, No. VS15TR22) at 1000 g/min for 10 min and washed with deionized H_2O three times, the obtained AgNPs were resuspended in deionized H_2O and stored at 4 °C.

2.2. Simulated Digestive Fluids

In vitro simulated digestion of AgNPs was performed according to a previous method.[32] The solutions of 1.25× concentration for simulated salivary fluid (SSF), simulated gastric fluid (SGF), and simulated intestinal fluid (SIF) were prepared by mixing the stock solutions (Table 1). The prepared solutions can be stored at −20 °C for 1 year or 2−5 °C for approximately 1 month. Before use, the necessary quantities of enzymes and Ca^{2+} solution would be added and finally diluted to a 1× concentration of the digestion fluids.

Table 1. Preparation of Simulated Digestive Fluids for the Oral, Gastric, and Intestinal Phase

			SSF (pH 7)	SGF (pH 3)	SIF (pH 7)
chemicals (1.25×)	concentrations		milliliters of stock added to prepare 10 mL (1.25×)	milliliters of stock added to prepare 20 mL (1.25×)	milliliters of stock added to prepare 20 mL
	(g/L)	(M)	(μL)	(μL)	(μL)
KCl	37.3	0.5	377.5	345	340
KH_2PO_4	68	0.5	92.5	45	40
$NaHCO_3$	84	1	170	625	2125
NaCl	117	2		590	480
$MgCl_2(H_2O)_6$	30.5	0.15	12.5	20	55
$(NH_4)_2CO_3$	48	0.5	1.5	25	
HCl		6	2.25	65	35
$CaCl_2(H_2O)_2$[a]	44.1	0.3	0.625	0.25	2

[a]$CaCl_2(H_2O)_2$ was added immediately before digestion.

2.3. Sequential Digestion of AgNPs Using a Simulated Semidynamic *In Vitro* Model

Figure 1 depicts an overview and flow diagram detailing the sequential digestion of AgNPs through a simulated semidynamic *in vitro* method, which was presented based on an international consensus developed by the COST INFOGEST network.[32] It is a static digestion method employing constant ratios of meals to digestive fluids and a constant pH at each phase of digestion. With this approach, samples undergo sequential oral, gastric, and intestinal digestion, with parameters such as electrolytes, enzymes, bile, pH, and time of digestion being based on available physiological data. According to the standardized protocol and dosages of AgNPs used in animal experiments,[32−35] a concentration of 1 mg/mL AgNPs was used in the simulated semidynamic *in vitro* model. The details about sequential digestion of AgNPs at respective phases are presented as follows:

2.3.1. Oral Phase. Pristine AgNPs (1 mL, 1 mg/mL, pAgNPs) were added into 1.25× 0.8 mL of SSF along with $CaCl_2(H_2O)_2$ (0.3 M, 5 μL) and deionized water (195 μL) to reach a final volume of 2

https://doi.org/10.1021/acsnanoscienceau.4c00012
ACS Nanosci. Au 2024, 4, 327−337

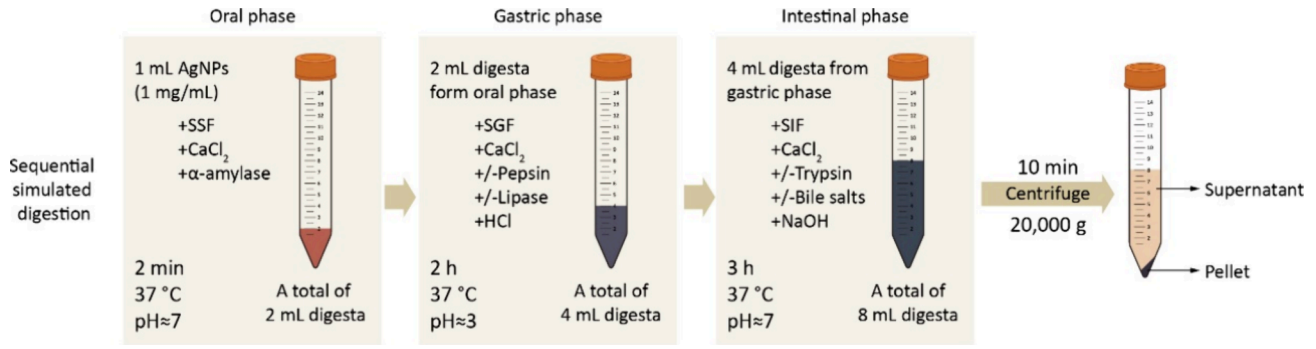

Figure 1. Overview and flow diagram of sequential digestion of AgNPs using a simulated *in vitro* semidynamic model with simulated salivary fluid (SSF), simulated gastric fluid (SGF), and simulated intestinal fluid (SIF).

Table 2. A Typical Sequential Digestion of Pristine AgNPs Using the Simulated Semidynamic *In Vitro* Protocol

	1 mL AgNPs				
input digestion phase	oral (SSF)	gastric (SGF)		intestinal (SIF)	
AgNPs or digesta	AgNPs	2 mL from the oral phase		4 mL from the gastric phase	
1.25× electrolyte stock solutions (mL)	0.8	1.6		1.6	
$CaCl_2(H_2O)_2$ (0.3 M) (μL)	5	1		8	
enzymes	α-amylase	pepsin	lipase	trypsin	bile salts
enzyme activity	75 U/mL	2000 U/mL	60 U/mL	100 U/mL	10 mM
volume of enzyme/bile to be added (mL)	0.15	0.133	0.096	1	0.6
H_2O (mL)	0.18	0.09		0.632	
HCl (5 M) for pH adj. (mL)		0.08			
NaOH (5 M) for pH adj. (mL)				0.16	
final volume (mL)	2	4		8	

mL (Table 2). α-Amylase was added to this reaction at 75 U/mL. Then, the digestion of AgNPs in this mixture was carried out for 2 min at 37 °C at pH 7.0.

2.3.2. Gastric Phase. Subsequently, 1.6 mL of 1.25× SGF with or without the inclusion of enzymes (2000 U/mL of pepsin and 60 U/mL of lipase) was added into the 2 mL oral digesta followed by the addition of 1 μL $CaCl_2(H_2O)_2$ (0.3 M). The pH was then adjusted to 3.0 with diluted HCl solution, and deionized water was subsequently added to achieve a final volume of 4 mL. This digestion was performed at 37 °C for 2 h in a water bath.

2.3.3. Intestinal Phase. A 1.6 mL portion of 1.25× SIF with or without the addition of 100 U/mL of trypsin and 10 mM of bile salts was added to 4 mL of gastric digesta. Subsequently, 1 μL $CaCl_2(H_2O)_2$ solution (0.3 M) was added into the mixture, and diluted NaOH solution was utilized to adjust the pH to 7.0, with a final volume of 8 mL. This mixture was incubated at 37 °C for 3 h.

All enzymes used in the digestion phase were prepared with the corresponding SSF, SGF, or SIF stock solution. The digested AgNPs without enzymes were named stAgNPs (enzymes−), whereas those with enzymes were referred to as estAgNPs (enzymes+). The sediments obtained from the final digestion phase were centrifuged at 20,000 g/min for 10 min and washed three times with deionized water under the same conditions. Finally, the digested AgNPs were resuspended in deionized H_2O for the subsequent experiments.

2.4. Transmission Electron Microscopy

The morphology and particle size of pristine AgNPs (pAgNPs), stAgNPs, and estAgNPs were determined using a transmission electron microscopy (TEM, JEM-2100F, JEOL, Japan). Briefly, a volume of 10 μL suspension was dropped onto a copper mesh (200 mesh, carbon film, China Mirror Science Instrument, China), left to dry completely, and observed at a magnification of 60,000×. Bright field images were acquired with TEM operating at a 200 kV accelerating voltage. Energy dispersive spectroscopy (EDS) mapping of pAgNPs, stAgNPs, and estAgNPs was performed on the same microscope equipped with an Oxford Ultim Max system (Oxford, UK). The diameter of the nanoparticles was measured using the software Nano Measurer 1.2.5.

2.5. Ultraviolet and Visible Spectrophotometry

The spectra of pAgNPs, stAgNPs, and estAgNPs were recorded using a DU-800 UV−vis spectrophotometer (Beckman, USA) within the wavelength range of 300 to 700 nm in deionized water.

2.6. Hydrodynamic Diameter and Zeta-Potential Assay

The hydrodynamic diameter and zeta potential of AgNPs were determined through dynamic light scattering (DLS) using a Nanosizer (NS90, Malvern, UK). Before each measurement, the samples were diluted to approximately 50 μg/mL with deionized water.

2.7. Cell Culture

Human colon epithelial cell line, Caco-2, was obtained from the American Type Culture Collection (ATCC, Manassas, USA). Cells were cultured in Dulbecco's modified Eagle medium (DMEM, Gibco, New York, USA) supplemented with 10% (v/v) fetal bovine serum (FBS, Invitrogen, Chicago, USA) and 1% (v/v) penicillin/streptomycin (Gibco, New York, USA) in a humidified atmosphere with 5% (v/v) CO_2 atmosphere at 37 °C. After reaching ∼80% confluence, cells were subcultured by washing three times with PBS (Solarbio, Beijing, China) and detaching by 0.25% (v/v) trypsin (Solarbio, Beijing, China).

2.8. Cell Viability

The cytotoxicity of AgNPs was determined by using the CCK-8 reagent (Dojindo, Tokyo, Japan). In details, cells were seeded in a 96-well plate at a density of 1×10^4 cells per well. After overnight incubation at 37 °C, the culture medium was supplemented with AgNPs at concentrations of 0, 5, 10, 20, or 40 μg/mL. After being exposed for 24 h, the culture medium containing AgNPs was removed, and cells were washed three times with PBS. Then, 10% (v/v) of stock CCK-8 reagent in FBS-free culture medium was added to each well and incubated for 2 h. Finally, the OD_{450} value was measured using a microplate reader (TECAN, Infinite 200 pro, Switzerland).

https://doi.org/10.1021/acsnanoscienceau.4c00012
ACS Nanosci. Au 2024, 4, 327−337

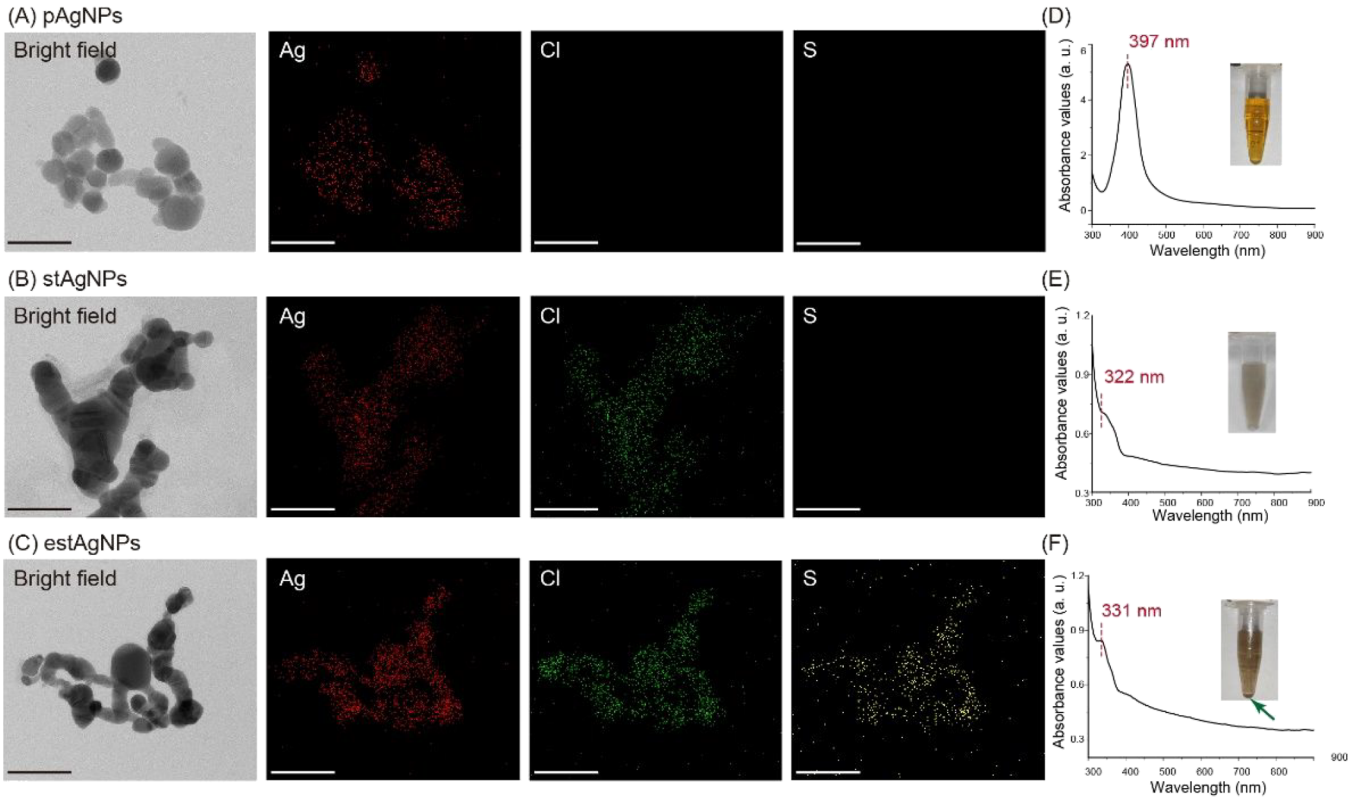

Figure 2. Transformation of AgNPs through *in vitro* gastrointestinal digestion. (A−C) TEM-EDS mapping of pAgNPs, stAgNPs, and estAgNPs. Scale bar: 100 nm. (D−F) Absorption spectra and photographs of pAgNPs, stAgNPs, and estAgNPs in deionized water.

2.9. Reactive Oxygen Species Assay

Cells were seeded in a 96-well plate at a density of 1×10^4 cells per well and incubated overnight. After removing the culture medium, cells were exposed to AgNPs at concentrations of 0, 10, 20, or 40 μg/mL for 24 h. Subsequently, the culture medium containing AgNPs was removed, and the cells were washed with PBS for three times. The cells were then incubated with 100 μL of a 5 μM DCFH-DA solution (Solarbio, Beijing, China, CA1410) for 30 min in the dark. As the positive control, 1% of hydrogen peroxide (H_2O_2) solution was used. Finally, the fluorescent intensity was determined with the microplate reader (TECAN, Infinite 200 pro, Switzerland) at excitation/emission wavelengths of 488/520 nm, respectively.

2.10. ICP-MS Analysis

2.10.1. Quantification of pAgNPs, stAgNPs, and estAgNPs. A volume of 50 μL of freshly prepared pAgNPs or sequentially digested stAgNPs or estAgNPs was mixed with 950 μL of digestion solution containing nitric acid (Sinopharm, China) and hydrogen peroxide (Sinopharm, China) at a ratio of 3:1 to reach a final volume of 1 mL. Following a 12 h digestion at room temperature, 100 μL of the resulting solution was diluted to 4 mL and then analyzed using ICP-MS (Agilent 8800, USA) for quantification.

2.10.2. Silver ion (Ag^+) Release of Sequentially Digested AgNPs through Different Phases. A volume of 1 mL of stAgNPs or estAgNPs at the end of each digestion phase (oral, gastric, and intestinal) was added to the centrifugation filter (Millipore, MWCO: 10 kDa, Shanghai, China) and ultrafiltrated at 3000 g/min for 5 min. Then, 100 μL filtrate was collected and diluted to 4 mL using 5% HNO_3 solution for ICP-MS analysis. Pristine AgNPs, which were not subjected to sequential digestion and underwent the same centrifugation procedure as the aforementioned samples, were utilized as the control.

2.10.3. Cellular Ag after Being Exposed to pAgNPs, stAgNPs, or estAgNPs. Cells were seeded in six-well plates at a density of 3×10^5 cells per well and allowed to adhere for 8 h. Subsequently, cells were exposed to different concentrations (0, 10, 20, or 40 μg/mL) of pAgNPs, stAgNPs, or estAgNPs. After 24 h, cells were washed three times with PBS and then digested with 1 mL of digestion solution containing nitric acid and hydrogen peroxide at a ratio of 3:1. After being digested at room temperature for 12 h, samples were diluted with 5% HNO_3 for ICP-MS measurement. At the same time, cells exposed in parallel were used to determine the protein concentration with the BCA kit (PC0020, Solarbio, China), which were subsequently used to normalize the Ag/protein ratios.

2.11. Metabolomics Analysis

Cells were seeded in a 10 cm Petri dish at a density of 2×10^6 cells per dish. After being incubated overnight, cells were exposed to pAgNPs, stAgNPs, or estAgNPs at a concentration of 0 or 20 μg/mL, respectively. After 24 h, cells were collected with a sterile scraper and centrifuged at 1000*g* for 3 min followed by three washes. Then, 300 μL of methanol (Fisher Chemical, USA) was added to the cell pellets, which were then sonicated for 5 min (350 W, QSONICA, Q500, USA) and centrifuged at 12,000 rpm for 10 min. Subsequently, 100 μL of the supernatant was introduced to LC−MS/MS (Vanquish, Thermo Fisher, USA) analysis. For the LC−MS/MS quantification, the chromatographic conditions were as follows: chromatographic column: Waters HSS T3 1.7 μm 2.1 × 100 mm (Waters, USA), column temperature: 40 °C, mobile phase A: 0.1% formic acid (Fisher Chemical, USA), mobile phase B: methanol, and flow rate: 0.3 mL/min. The mass spectrometry conditions were as follows: primary mass spectrometry parameters: resolution: 70,000, AGC target: 1e6, maximum IT: 50 ms, scan range: 150 to 1500 m/z; secondary mass spectrometry parameters: resolution: 17,500, AGC target: 1e5, maximum IT: 50 ms, TopN: 10, and NCE/stepped NCE: 10, 30, 55. The obtained mass spectra were searched and matched to determine the relative content of the molecules. The main process included (1) conversion of the raw data obtained by LC−MS into ABF format through the Analysis Base File Converter software (ver 4.48); (2) importation of the ABF format file into MS-DIAL 4.70[36] (MS-DIAL: data independent MS/MS deconvolution for comprehensive metabolome analysis; the software performed preprocessing,

https://doi.org/10.1021/acsnanoscienceau.4c00012
ACS Nanosci. Au 2024, 4, 327−337

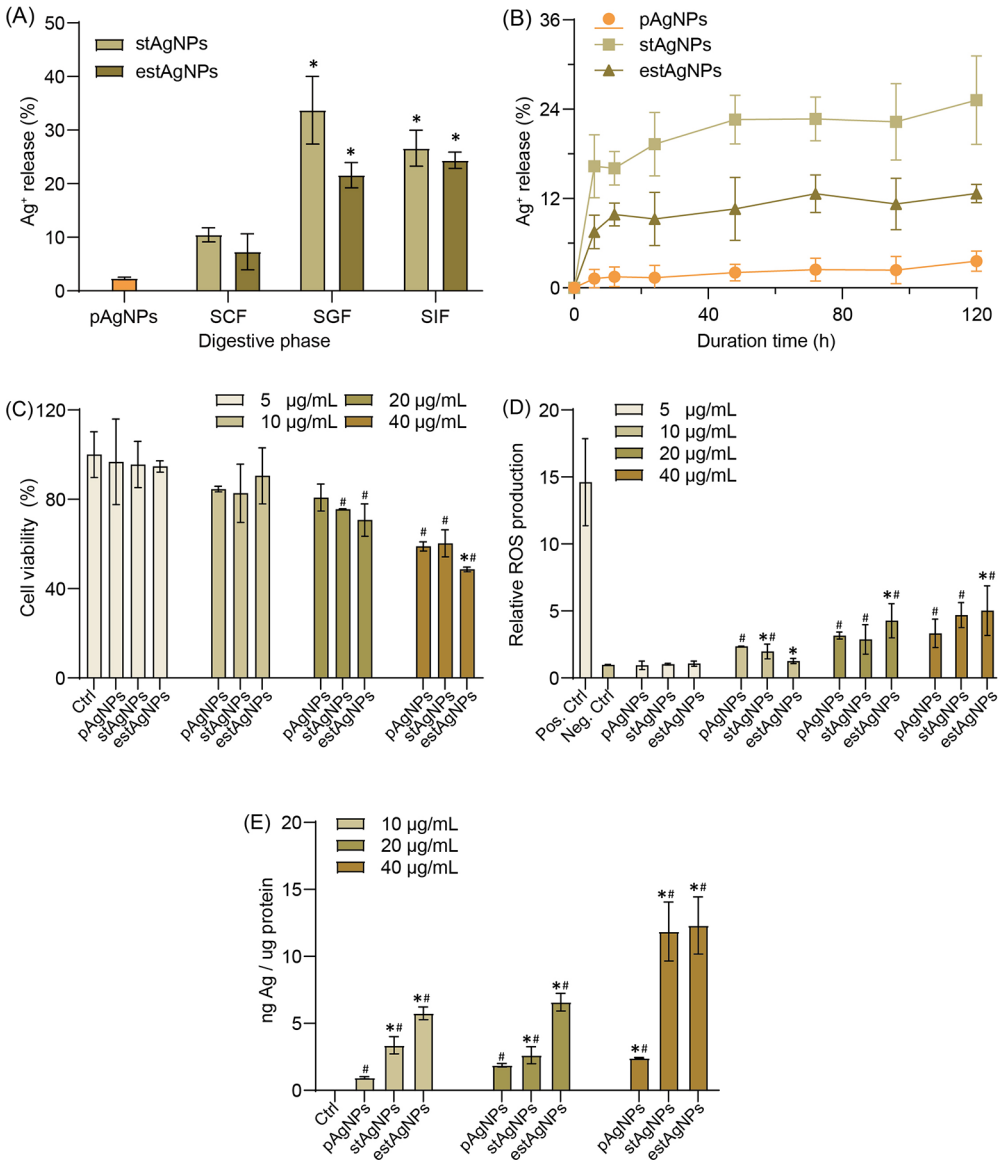

Figure 3. Release of $Ag^+$from AgNPs during sequential digestion and cytotoxicity in enterocytes. (A) Release of Ag^+ from stAgNPs and estAgNPs at each stage of digestion determined with ICP-MS (n = 6). (B) Release of Ag^+ from pAgNPs, stAgNPs, and estAgNPs in deionized water over 120 h (n = 6). (C) Cell viability after being exposed to pAgNPs, stAgNPs, and estAgNPs at 0, 5, 10, 20, and 40 μg/mL for 24 h (n = 3). (D) ROS generation induced by pAgNPs, stAgNPs, and estAgNPs (n = 5). Caco-2 cells treated with 1% H_2O_2 are used as the positive control. (E) Ag in cells after being exposed to pAgNPs, stAgNPs, and estAgNPs at 0, 10, 20, and 40 μg/mL for 24 h (n = 3). The symbol "*" indicates a P value < 0.05 compared to pAgNPs, whereas the symbol "#" indicates a P value < 0.05 compared to the "Ctrl" group.

including peak extraction, noise removal, deconvolution, and peak alignment, and exported a three-dimensional data matrix (original data matrix) in CSV format); and (3) comparison of the extracted peak information and full database search using MassBank, Respect, and GNPS. This matrix included information such as sample details, retention time, mass-to-charge ratio, and mass spectrum response intensity (peak area). The final substance information obtained after database search and matching included average Rt (min), average Mz, metabolite name, adduct type, reference m/z, formula, ontology, MS1 isotope, MSMS spectrum, etc.

2.12. Statistical Analysis

All data were expressed as the mean ± the standard deviation (SD). Statistical analysis was conducted by the Statistical Package for the Social Sciences (SPSS), version 18.0 (SPSS Inc., Chicago, IL, USA). The difference between the single treated group and the control group was determined using an independent t test. The significance of the mean difference for two or more treated groups relative to the control group was analyzed by a one-way analysis of variance (ANOVA) test. P < 0.05 was considered statistically significant.

3. RESULTS AND DISCUSSIONS

3.1. Physicochemical Changes of AgNPs Digested with an *In Vitro* Gastrointestinal Digestion Model

To investigate the transformation of AgNPs throughout the oral, gastric, and intestinal phases, pAgNPs were treated using the *in vitro* gastrointestinal digestion model without or with digestive enzymes, resulting in the formation of stAgNPs (enzyme−) and estAgNPs (enzyme+). The diameter of pAgNPs was determined to be 23.14 ± 3.83 nm (Figure S1). After sequential digestion, stAgNPs and estAgNPs exhibited a tendency to aggregate into larger particles with the size of 85.78 ± 31.90 and 100.17 ± 33.57 nm, respectively. Similarly, the hydrodynamic diameter of stAgNPs and

https://doi.org/10.1021/acsnanoscienceau.4c00012
ACS Nanosci. Au 2024, 4, 327−337

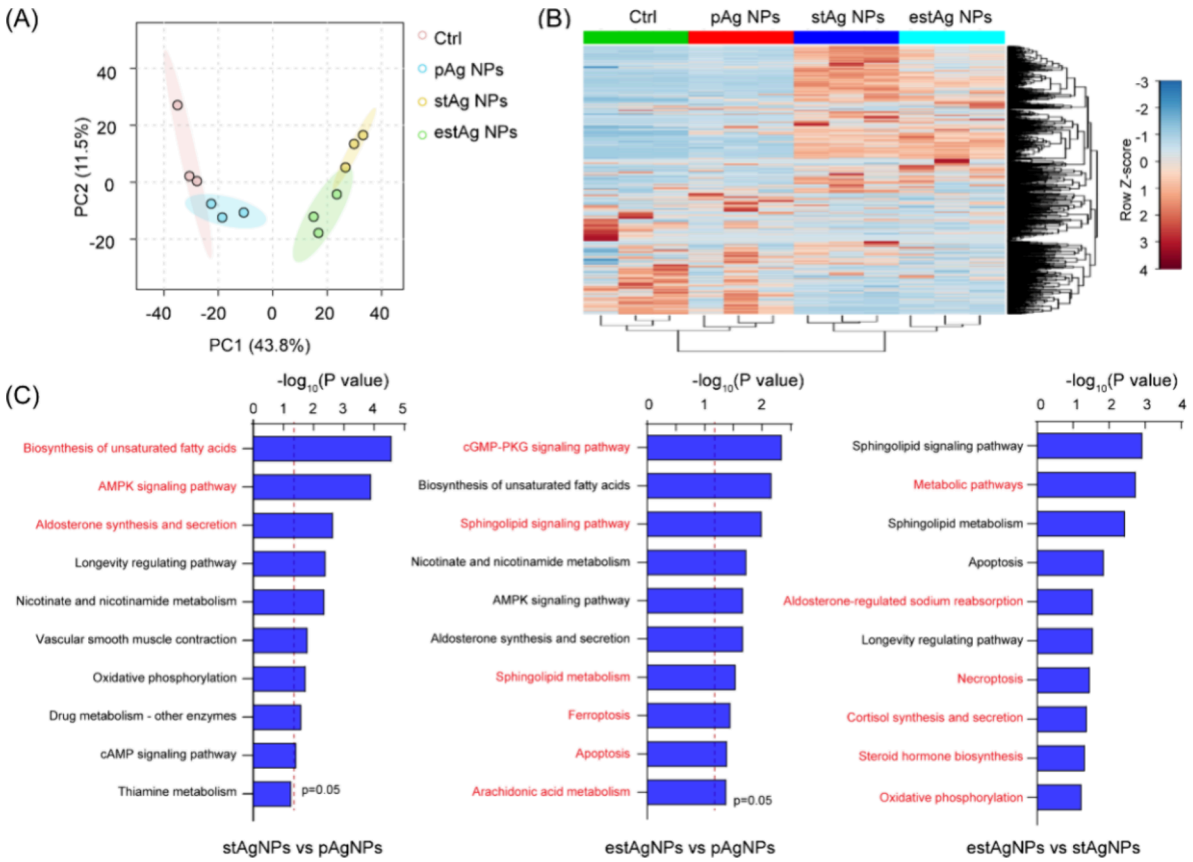

Figure 4. Metabolomic profiles of enterocytes after being exposed to pAgNPs, stAgNPs, or estAgNPs. (A) Principal component analysis (PCA) of metabolites for the cells treated with AgNPs (pAgNPs, stAgNPs, and estAgNPs) and untreated cells (n = 3). (B) Hierarchical clustering analysis (HCA) of metabolites. (C) Enriched metabolic pathway of differentially changed metabolites (DCMs) in the stAgNP vs pAgNP group, estAgNP vs pAgNP group, and estAgNP vs stAgNPs AgNP group.

estAgNPs was determined to be 183.98 ± 22.58 and 302.45 ± 46.57 nm, confirming the significant aggregation of pAgNPs (Figure S2). Furthermore, we performed elemental mapping to examine the chemical composition of the pAgNPs, stAgNPs, and estAgNPs. TEM-EDS images show that stAgNPs have an obvious colocalization of Ag and Cl, whereas Ag coexists with Cl and S in estAgNPs (Figure 2 and Figure S2). The presence of Cl^- in the electrolytes is expected to lead to the formation of Ag−Cl species.[25] It is reported that Cl^- in the aqueous phase can facilitate the aggregation of AgNPs through reducing the electrostatic repulsion between particles.[37] On the other side, digestive enzymes in the GIT may form protein corona on the particles,[38] which may alter the tendency of AgNPs to aggregate, which in turn changes the physicochemical properties of AgNPs. As observed, the colloidal solution of pAgNPs exhibits an orange color, displaying a distinct plasmonic peak at the wavelength of 397 nm, which experienced a blueshift to 322 nm for stAgNPs and 331 nm for estAgNPs after sequential digestion, suggesting a significant transformation of AgNPs during digestion. Additionally, obvious sedimentation was observed for estAgNPs (the green arrow in Figure 2F), indicating that the electrolytes and enzymes induced complicated structural changes of AgNPs. Taken together, *in vitro* digestion can promote AgNPs to undergo complex chemical and biological transformations, which are crucial for assessing the toxicity of AgNPs *in vivo*.

3.2. Dissolution and Cytotoxicity of AgNPs in Digestive Fluids

The sequentially digested AgNPs underwent significant alterations in particle size, zeta potential, and structure, but the dissolution of AgNPs at different phases in the GIT remains a mystery due to variations in pH, enzymes, and other components.[10,11] To unveil the possible mechanisms, the supernatants obtained at the end of each phase during digestion were gathered and subjected to analysis of the release of Ag^+ from AgNPs with ICP-MS. As shown in Figure 3A, compared with pAgNPs, both stAgNPs and estAgNPs had more Ag^+ release in three digestion phases, especially in SGF (pH 3) and SIF (pH 7). Previous studies showed that, in acidic solutions, oxidation dissolution may occur on the surface of AgNPs, resulting in the release of Ag^+.[39] Alternatively, digestive enzymes such as α-amylase, gastric pepsin, gastric lipase, and pancreatic trypsin can interact with AgNPs, driven by hydrophobic and electrostatic interactions, thereby stabilizing or destabilizing the particles.[25,40−44] It can explain why estAgNPs had less Ag^+ release compared to that of stAgNPs in three digestive phases (7.29 vs 10.47% in the oral phase, 21.58 vs 33.73% in the gastric phase, and 24.37 vs 26.62% in the intestinal phase). These findings also suggest that the gastric and intestinal conditions serve as the primary sites for the digestion of AgNPs in the GIT, which is markedly influenced by the acidic condition, ions, and enzymes in digestive fluids.[45,46] Moreover, there was a sustained release of nearly 20% Ag^+ over a period of 120 h for stAgNPs, whereas

https://doi.org/10.1021/acsnanoscienceau.4c00012
ACS Nanosci. Au 2024, 4, 327−337

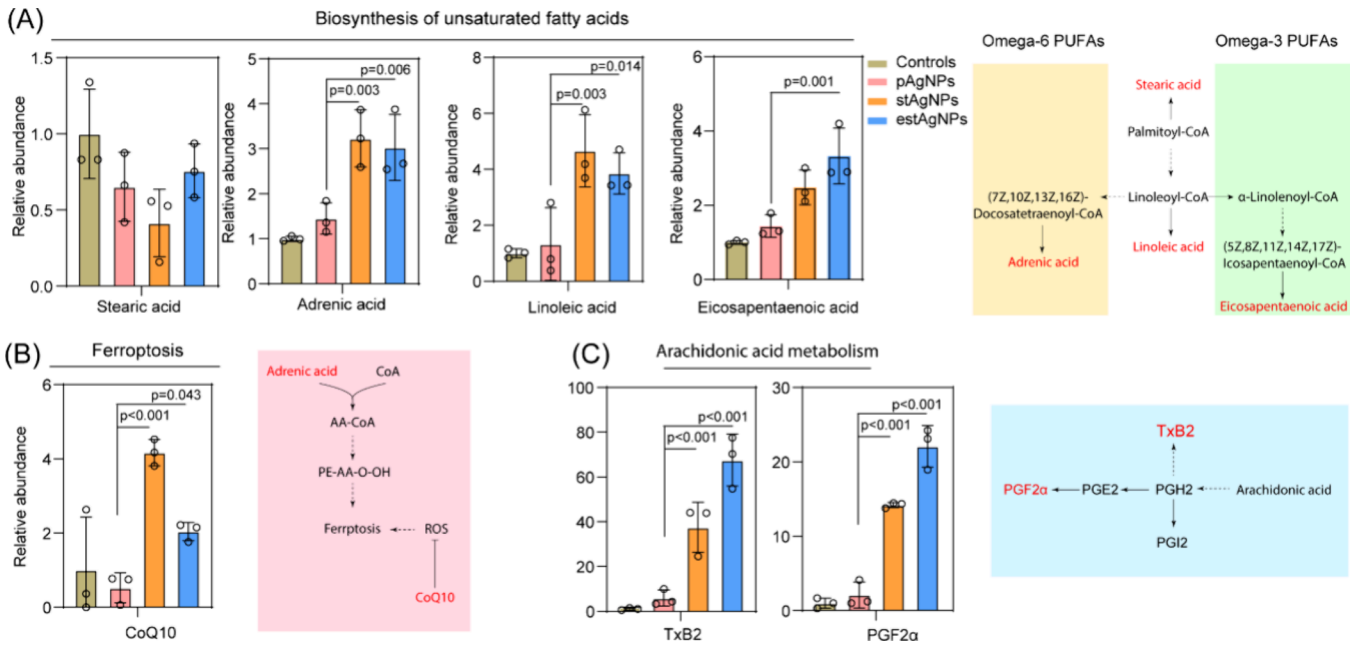

Figure 5. Metabolic pathway analysis. Changes of DCMs and corresponding pathway map of (A) biosynthesis of unsaturated fatty acid, (B) ferroptosis, and (C) arachidonic acid metabolism. CoQ10, ubiquinone-10; TxB2, thromboxane B2; PGF2α, prostaglandin F2alpha; PGI2, prostaglandin I2 (n = 3). The symbol "*" indicates a P value < 0.05 compared with stAgNPs and estAgNPs to pAgNPs, whereas the symbol "#" represents a P value < 0.05 compared to the "Ctrl" group.

that for estAgNPs and pAgNPs is less than 10 and 5%, respectively (Figure 3B).

Numerous studies have demonstrated that the cytotoxicity of AgNPs primarily comes from the release of Ag^+ dissolved from particles.[47] Thus, to reveal the cytotoxicity of sequentially digested AgNPs in enterocytes, Caco-2 cells were employed. As depicted in Figure 3C, the cell viability of pAgNPs, stAgNPs, and estAgNPs declined in a dose-dependent manner. Notably, the decrease in cell viability induced by estAgNPs was slightly higher than that of stAgNPs and pAgNPs, especially at a concentration of 40 μg/mL. Additionally, we also observed that ROS generation induced by all three types of AgNPs exhibited a dose-dependent increase. The highest level of ROS caused by estAgNPs is nearly two times higher than that of pAgNPs at a concentration of 40 μg/mL (Figure 3D). These findings were consistent with the cellular uptake of AgNPs (Figure 3E). The uptake of Ag in cells treated with pAgNPs, stAgNPs, and estAgNPs also exhibited a dose-dependent increase, with the highest uptake observed in estAgNPs-treated cells followed by stAgNPs and pAgNPs. The Ag content in estAgNPs-treated cells was 6.58 ng/μg protein, which is higher than that of pAgNPs and stAgNPs, suggesting that estAgNPs were more readily taken up by Caco-2 cells. Previous studies have revealed that the cytotoxicity of AgNPs can be affected by their surface coating, Ag^+ release, and cellular uptake.[48,49] Our results suggest that particle aggregation may be another important factor contributing to the cytotoxicity of AgNPs in the GIT, as there is less Ag^+ release from estAgNPs compared to that from pAgNPs and stAgNPs. Moreover, the protein corona formed on AgNPs may alter their interactions with cells.[50] Previous studies using gastrointestinal fluids to incubate AgNPs for *in vitro* cell experiments also demonstrated that near-neutral pH and high concentrations of salt increased the release of Ag^+ from AgNPs, consequently enhancing their cellular uptake.[51,52] In addition, bile salt in the GIT was found to potentially disrupt the tight structure of monolayer Caco-2 cells (e.g., reduction of TEER and ROS production, in consistent with our cytotoxicity tests), resulting in an imbalance in energy metabolism and redox homeostasis in Caco-2 cells.[53] It may be attributed to metabolic dysfunction via numerous enzymes such as PLA2 (phospholipase A2), COX (cyclooxygenase), PKC (protein kinase), ERK 1/2 (extracellular signal-regulated kinase 1/2), PI 3 K (phosphatidylinositol 3-kinase), p38 MAPK (p38 mitogen-activated protein kinase), MLCK (myosin light-chain kinase), NADH dehydrogenase, and XO (xanthine oxidase).[53] However, the specific cellular uptake and resulting cytotoxicity need to be further elucidated. Overall, during the *in vitro* sequential digestion process, AgNPs tend to aggregate, and the presence of digestive enzymes and high concentrations of salt increases the cellular uptake of Ag, ultimately leading to the elevated ROS generation and cytotoxicity.

3.3. Metabolomic Profiles of Enterocytes in Response to Digested AgNPs

To comprehensively reveal the toxicological mechanisms of sequentially digested AgNPs in enterocytes, the profiles of differentially changed metabolites (DCMs) were determined through metabolomics analysis. The score plots of PCA show a clear separation between cells treated with AgNPs (pAgNPs, stAgNPs, and estAgNPs) and untreated cells (Figure 4A). The first two principal components (PC1 and PC2) of metabolites accounted for 43.8% and 11.5% of the total metabolites, respectively, indicating a large degree of variance in the metabolites between cells treated with AgNPs (pAgNPs, stAgNPs, and estAgNPs) and untreated cells. In addition, there is a significant separation between cells treated with AgNPs (pAgNPs, stAgNPs, and estAgNPs) and untreated cells, in consistent with the PCA results (Figure 4B). The clustering heatmap shows that sequentially digested AgNPs (stAgNPs and estAgNPs) enhanced and repressed the production of some metabolites in Caco-2 cells compared

https://doi.org/10.1021/acsnanoscienceau.4c00012
ACS Nanosci. Au 2024, 4, 327−337

with pAgNPs and untreated cells. Meanwhile, the estAgNPs-treated cells induced altercations of some metabolites in a way comparable with that of stAgNPs. In summary, the cluster heatmap demonstrates dramatic differences in the metabolite profiles of enterocytes treated with AgNPs of different types. Furthermore, KEGG enrichment analysis was performed to further investigate the pathways or biological processes resulting from the sequentially digested AgNPs. For the pAgNPs vs control group, only the pathway of "pyrimidine metabolism" was significantly enriched ($P < 0.05$) (Figure S3C). Recent studies suggest its important role in cellular processes induced by AgNPs, such as energy metabolism, cell proliferation, and growth.[54] Notably, stAgNPs and estAgNPs induced significant metabolic alterations, mainly associated with the "biosynthesis of unsaturated fatty acids", "central carbon metabolism in cancer", the "AMPK signaling pathway", the "biosynthesis of amino acids", "nicotinate and nicotinamide metabolism", and "ferroptosis". It implies that pAgNPs, after sequential digestion in the GIT, can disturb various metabolic processes, including lipid metabolism, metabolic pathway, and cell survival. Furthermore, we also compared the pathway alteration of DCMs between pAgNPs, stAgNPs, and estAgNPs (Figure 4C). For the stAgNP vs pAgNP group, DCMs mainly enrich in the "biosynthesis of unsaturated fatty acids", suggesting significant alterations in metabolic pathways associated with lipid metabolism in response to stAgNPs. Regarding the estAgNP vs pAgNP group, besides the above pathway, more significant pathways are enriched, including the "cGMP-PKG signaling pathway", the "sphingolipid signaling pathway", the "sphingolipid metabolism", "ferroptosis", and "apoptosis". Additionally, we found that the "metabolic pathways", "aldosterone-regulated sodium reabsorption", and "necroptosis" were enriched in the estAgNP vs stAgNP group. These findings were consistent with the above results, confirming that the biological process induced by sequentially digested AgNPs was more significant than that of pAgNPs. As reported, ROS can affect fatty acid anabolism and unsaturated fatty acid synthesis by oxidizing lipids and regulating fatty acid synthase activity which in turn directly or indirectly activate ferroptosis.[55]

3.4. Metabolomics Analysis to Reveal Ferroptosis Induced by Digested AgNPs in Enterocytes

To clarify the mechanisms of cytotoxicity induced by sequentially digested AgNPs, we specifically analyzed the abundance of DCMs enriched in these pathways and depicted their pathway map. Regarding the biosynthesis of unsaturated fatty acids (UFAs) (Figure 5A), sequentially digested estAgNPs primarily caused a remarkable upregulation of adrenic acid, linoleic acid, and eicosapentaenoic acid than pAgNPs. Adrenic acid (AdA, 22:4) is the one of the representative species of the omega-6 series of polyunsaturated fatty acids, mainly formed through a two-carbon chain elongation of arachidonic acid (ARA) or through elongation and desaturation of linoleic acid.[56] In addition, eicosapentaenoic acid (EPA, 20:5) is an omega-3 fatty acid, which can be converted by a portion of absorbed alpha-linolenic acid. Linolenic acid and alpha-linolenic acid are essential fatty acids in the human body, and both of them can be converted into each other. As shown in Figure 5A, we observed an elevated level of linoleic acid. These findings indicate that sequentially digested Ag NPs, especially estAgNPs, can disorder the lipid metabolism, leading to an increase of ARA and EPA mediated linolenic acid. It has been reported that EPA is a beneficial fatty acid that can alleviate and regulate inflammation.[57] Nevertheless, the high degree of unsaturation of AdA renders it vulnerable to oxidation, leading to the formation of lipid peroxides and subsequently increasing the risk of ferroptosis.[58] Ferroptosis is a form of regulated cell death characterized by the iron-dependent accumulation of lipid peroxides to lethal levels.[59] Ubidecarenone-10 CoQ10, an important intracellular antioxidant, is involved in scavenging free radicals and attenuating oxidative stress, thereby inhibiting the onset of ferroptosis.[60] As shown in Figure 5B, CoQ10 was significantly altered by stAgNPs and estAgNPs compared with pAgNPs, indicating the potential occurrence of ferroptosis. However, our result demonstrated the increase of both CoQ10 and ROS, indicating the imbalance of the antioxidant system or impaired mitochondrial function. Therefore, further studies are necessary to understand the underlying mechanism and take corresponding measures to restore the intracellular redox homeostasis.[61] Another important initiation of ferroptosis is arachidonic acid (AA), which is a polyunsaturated omega-6 fatty acid 20:4, present in the phospholipids (especially phosphatidylethanolamine, phosphatidylcholine, and phosphatidylinositides) of cell membranes.[62] AA released after cell activation is catalyzed by acyl-coenzyme A synthetases long-chain isoform (ACSL) metabolized into various bioactive lipid mediators involved in ferroptosis.[63] Notably, AA can be catalyzed by cyclooxygenase (COX) to form a transitional epoxy precursor, which is then converted to thromboxane B2 (TxB2) by TxB2 synthase and prostaglandin F2alpha (PGF2α) by PGF2α synthase, involving the regulation of cell biological process. In Figure 5C, we found that TxB2 and PGF2α were highly elevated almost dozens of times compared to pAgNPs, suggesting the disorder of AA metabolism. In summary, sequentially digested AgNPs mainly manifested in the disorder of lipid metabolism and disruption of the ferroptosis pathway via the regulation of AdA- and AA-related metabolites. These metabolomic alterations are closely related with the physicochemical properties of three types of AgNPs. The size- and surface-dependent uptake of nanoparticles encompassed with gastrointestinal enzymes and salts, mediated by endocytosis, might exacerbate the cytotoxicity of the nanoparticles by affecting their metabolic pathways.[64−67] These findings provide valuable information for understanding the toxicological mechanism of AgNPs in the GIT.

CONCLUSIONS

In summary, we investigated the physicochemical changes in the sequential digestion of AgNPs and analyzed their cytotoxicity in enterocytes through metabolomics analysis. Specifically, our results indicate that AgNPs, throughout an *in vitro* sequential digestion from the oral, gastric, and intestinal phases, tended to aggregate and form a larger size because of Ag−Cl and Ag−S interactions. However, under acidic conditions, sequentially digested AgNPs were prone to dissolve and release Ag^+. And the presence of digestive enzymes and high concentrations of salt increases the cellular uptake of Ag, ultimately leading to more ROS generation and disordered lipid metabolism. The disorder of unsaturated fatty acid metabolism and alteration of CoQ10 may activate ferroptosis in AgNP-treated cells. Our study reveals the physicochemical alterations of sequential digested AgNPs through *in vitro* simulation of gastrointestinal digestion and the resulting metabolomic profiles in enterocytes, which closely mimic the

https://doi.org/10.1021/acsnanoscienceau.4c00012
ACS Nanosci. Au 2024, 4, 327−337

real GIT conditions, which is helpful to understand the health risks of AgNPs ingested orally.

■ ASSOCIATED CONTENT

Data Availability Statement

All other data supporting the findings of this study are available within the article and the Supporting Information files.

Supporting Information

The Supporting Information is available free of charge at https://pubs.acs.org/doi/10.1021/acsnanoscienceau.4c00012.

Representative TEM images, hydrodynamic diameter and zeta (ζ) potential, and EDX spectra of pAgNPs, stAgNPs, and estAgNPs; enriched metabolic pathway of differentially changed metabolites (DCMs) in the pAgNPs vs control group, stAgNPs vs control group, and estAgNPs vs control group; and all metabolic pathways enriched in the three groups of AgNPs in Table S1 (PDF)

■ AUTHOR INFORMATION

Corresponding Author

Ruixia Wang − *State Key Laboratory of Environmental Chemistry and Ecotoxicology, Research Center for Eco-Environmental Sciences, Chinese Academy of Sciences, Beijing 100085, China; College of Resources and Environment, University of Chinese Academy of Sciences, Beijing 100049, China;* orcid.org/0009-0007-1504-921X; Email: rxwang_st@rcees.ac.cn

Authors

Yongjiu Chen − *Key Laboratory of Carcinogenesis and Translational Research (Ministry of Education/Beijing), Unit III & Ostomy Service, Gastrointestinal Cancer Center, Peking University Cancer Hospital & Institute, Beijing 100142, China*

Ming Xu − *State Key Laboratory of Environmental Chemistry and Ecotoxicology, Research Center for Eco-Environmental Sciences, Chinese Academy of Sciences, Beijing 100085, China; College of Resources and Environment, University of Chinese Academy of Sciences, Beijing 100049, China;* orcid.org/0000-0002-4499-6116

Complete contact information is available at: https://pubs.acs.org/10.1021/acsnanoscienceau.4c00012

Author Contributions

Yongjiu Chen: conceptualization; methodology; formal analysis; writing − original draft; funding acquisition. Ruixia Wang: conceptualization; formal analysis; supervision; draft revision; funding acquisition. Ming Xu: project administration. CRediT: **Yongjiu Chen** conceptualization, formal analysis, funding acquisition, methodology, software, validation, writing-original draft; **Ruixia Wang** conceptualization, formal analysis, funding acquisition, supervision, writing-original draft; **Ming Xu** project administration.

Funding

This study is supported by the National Natural Science Foundation of China (22206006, 22306194, 22376211).

Notes

The authors declare no competing financial interest.

■ ACKNOWLEDGMENTS

The authors would like to thank Dr. Lining Xu and Mrs. Fanglan Geng from the State Key Laboratory of Environmental Chemistry and Ecotoxicology, Research Center for Eco-Environmental Sciences, Chinese Academy of Sciences, for the AgNP preparation and TEM analysis.

■ REFERENCES

(1) Chen, Y.; Ma, J.; Xu, M.; Liu, S. Antiviral nanoagents: More attention and effort needed? *Nano Today* **2020**, *35*, 1−11.

(2) Chaudhry, Q.; Scotter, M.; Blackburn, J.; Ross, B.; Boxall, A.; Castle, L.; Aitken, R.; Watkins, R. Applications and implications of nanotechnologies for the food sector. *Food additives and contaminants.* **2008**, *25*, 241−258.

(3) Verleysen, E.; Van Doren, E.; Waegeneers, N.; De Temmerman, P.-J.; Abi Daoud Francisco, M.; Mast, J. TEM and SP-ICP-MS analysis of the release of silver nanoparticles from decoration of pastry. *Journal of agricultural and food chemistry.* **2015**, *63*, 3570−3578.

(4) Larsen, P. B.; Christensen, F.; Jensen, K. A.; Brinch, A.; Mikkelsen, S. H. *Exposure assessment of nanomaterials in consumer products*. The Danish Environmental Protection Agency 2015, *32*, 2345−2348.

(5) Quadros, M. E.; Pierson, R., IV; Tulve, N. S.; Willis, R.; Rogers, K.; Thomas, T. A.; Marr, L. C. Release of silver from nanotechnology-based consumer products for children. *Environmental science & technology.* **2013**, *47*, 8894−8901.

(6) Mackevica, A.; Olsson, M. E.; Hansen, S. F. Silver nanoparticle release from commercially available plastic food containers into food simulants. *J. Nanopart. Res.* **2016**, *18*, 1−11.

(7) Jia, J.; Li, F.; Zhou, H.; Bai, Y.; Liu, S.; Jiang, Y.; Jiang, G.; Yan, B. Oral exposure to silver nanoparticles or silver ions may aggravate fatty liver disease in overweight mice. *Environmental science & technology.* **2017**, *51*, 9334−9343.

(8) Sofranko, A.; Wahle, T.; Heusinkveld, H. J.; Stahlmecke, B.; Dronov, M.; Pijnenburg, D.; Hilhorst, R.; Lamann, K.; Albrecht, C.; Schins, R. P. Evaluation of the neurotoxic effects of engineered nanomaterials in C57BL/6J mice in 28-day oral exposure studies. *Neurotoxicology.* **2021**, *84*, 155−171.

(9) Garcia, T.; Lafuente, D.; Blanco, J.; Sánchez, D. J.; Sirvent, J. J.; Domingo, J. L.; Gómez, M. Oral subchronic exposure to silver nanoparticles in rats. *Food Chem. Toxicol.* **2016**, *92*, 177−187.

(10) Wang, X.; Xu, L.; Ma, M.; Xu, M.; Zhou, Q.; Liu, S.; Jiang, G. A Novel Strategy for Visualizing, Tracing, and Measuring the Gastrointestinal Absorption of Silver Nanoparticles. *Adv. Funct. Mater.* **2023**, *33*, 1−9.

(11) Qi, M.; Wang, X.; Chen, J.; Liu, Y.; Liu, Y.; Jia, J.; Li, L.; Yue, T.; Gao, L.; Yan, B.; Zhao, B.; Xu, M. Transformation, Absorption and Toxicological Mechanisms of Silver Nanoparticles in the Gastrointestinal Tract Following Oral Exposure. *ACS Nano* **2023**, *17*, 8851−8865.

(12) Shahare, B.; Yashpal, M. Gajendra, Toxic effects of repeated oral exposure of silver nanoparticles on small intestine mucosa of mice. *Toxicology mechanisms and methods.* **2013**, *23*, 161−167.

(13) Kim, Y. S.; Song, M. Y.; Park, J. D.; Song, K. S.; Ryu, H. R.; Chung, Y. H.; Chang, H. K.; Lee, J. H.; Oh, K. H.; Kelman, B. J.; Hwang, I. K.; Yu, I. J. Subchronic oral toxicity of silver nanoparticles. *Part. Fibre Toxicol.* **2010**, *7*, 1−11.

(14) Ren, Q.; Ma, J.; Li, X.; Meng, Q.; Wu, S.; Xie, Y.; Qi, Y.; Liu, S.; Chen, R. Intestinal toxicity of metal nanoparticles: silver nanoparticles disorder the intestinal immune microenvironment. *ACS Applied Materials & Interfaces.* **2023**, *15*, 27774−27788.

(15) Narasimha, V. R.; Latha, T. S.; Pallu, R.; Panati, K.; Narala, V. R. Anticancer activities of biogenic silver nanoparticles targeting apoptosis and inflammatory pathways in colon cancer cells. *Journal of Cluster Science.* **2022**, *33*, 2215−2231.

(16) Sousa, A.; Azevedo, R.; Costa, V. M.; Oliveira, S.; Preguiça, I.; Viana, S.; Reis, F.; Almeida, A.; Matafome, P.; Dias-Pereira, P.;

Carvalho, F.; Fernandes, E.; Freitas, M. Biodistribution and intestinal inflammatory response following voluntary oral intake of silver nanoparticles by C57BL/6J mice. *Arch. Toxicol.* **2023**, *97*, 2643−2657.
(17) Sousa, A.; Bradshaw, T. D.; Ribeiro, D.; Fernandes, E.; Freitas, M. Pro-inflammatory effects of silver nanoparticles in the intestine. *Arch. Toxicol.* **2022**, *96*, 1551−1571.
(18) van Den Brule, S.; Ambroise, J.; Lecloux, H.; Levard, C.; Soulas, R.; De Temmerman, P.-J.; Palmai-Pallag, M.; Marbaix, E.; Lison, D. Dietary silver nanoparticles can disturb the gut microbiota in mice. *Part. Fibre Toxicol.* **2015**, *13*, 1−16.
(19) Li, M.; Zhang, C. Are silver nanoparticles better than triclosan as a daily antimicrobial? Answers from the perspectives of gut microbiome disruption and pathogenicity. *Science of The Total Environment.* **2021**, *756*, 143983−143988.
(20) Ghebretatios, M.; Schaly, S.; Prakash, S. Nanoparticles in the food industry and their impact on human gut microbiome and diseases. *International Journal of Molecular Sciences.* **2021**, *22*, 1942−1950.
(21) Lamas, B.; Breyner, N. M.; Houdeau, E. Impacts of foodborne inorganic nanoparticles on the gut microbiota-immune axis: potential consequences for host health. *Part. Fibre Toxicol.* **2020**, *17*, 1−22.
(22) Guan, Q. A comprehensive review and update on the pathogenesis of inflammatory bowel disease. *J. Immunol. Res.* **2019**, *2019*, 1−12.
(23) Beer, C.; Foldbjerg, R.; Hayashi, Y.; Sutherland, D. S.; Autrup, H. Toxicity of silver nanoparticles—nanoparticle or silver ion? *Toxicology letters.* **2012**, *208*, 286−292.
(24) De Matteis, V.; Malvindi, M. A.; Galeone, A.; Brunetti, V.; De Luca, E.; Kote, S.; Kshirsagar, P.; Sabella, S.; Bardi, G.; Pompa, P. P. Negligible particle-specific toxicity mechanism of silver nanoparticles: the role of Ag+ ion release in the cytosol. *Nanomedicine: Nanotechnology, Biology and Medicine.* **2015**, *11*, 731−739.
(25) Carnovale, C.; Guarnieri, D.; Di Cristo, L.; De Angelis, I.; Veronesi, G.; Scarpellini, A.; Malvindi, M. A.; Barone, F.; Pompa, P. P.; Sabella, S. Biotransformation of silver nanoparticles into oro-gastrointestinal tract by integrated in vitro testing assay: generation of exposure-dependent physical descriptors for nanomaterial grouping. *Nanomaterials.* **2021**, *11*, 1587−1596.
(26) Mwilu, S. K.; El Badawy, A. M.; Bradham, K.; Nelson, C.; Thomas, D.; Scheckel, K. G.; Tolaymat, T.; Ma, L.; Rogers, K. R. Changes in silver nanoparticles exposed to human synthetic stomach fluid: effects of particle size and surface chemistry. *Sci. Total Environ.* **2013**, *447*, 90−98.
(27) Abdelkhaliq, A.; van der Zande, M.; Undas, A. K.; Peters, R. J.; Bouwmeester, H. Impact of in vitro digestion on gastrointestinal fate and uptake of silver nanoparticles with different surface modifications. *Nanotoxicology.* **2020**, *14*, 111−126.
(28) Dupont, D.; Bordoni, A.; Brodkorb, A.; Capozzi, F.; Velickovic, T. C.; Corredig, M.; Cotter, P. D.; De Noni, I.; Gaudichon, C.; Golding, M.; Lea, T.; Le Huërou-Luron, I.; Mackie, A.; Madsen, C.; De Meulenaer, B.; Nys, Y.; Pihlanto, A.; Recio, I.; Rémond, D.; Requena, T.; Souchon, I.; Swiatecka, D.; Turgeon, S.; Vegarud, G.; Vreeburg, R.; Weitschies, W.; Wickham, M. An international network for improving health properties of food by sharing our knowledge on the digestive process. *Food Dig.* **2011**, *2*, 23−25.
(29) Wang, R.; Chen, Y.; Chen, J.; Ma, M.; Xu, M.; Liu, S. Integration of transcriptomics and metabolomics analysis for unveiling the toxicological profile in the liver of mice exposed to uranium in drinking water. *Environ. Pollut.* **2023**, *335*, 122296−122301.
(30) Vaccari, F.; Zhang, L.; Giuberti, G.; Grasso, A.; Bandini, F.; García-Pérez, P.; Copat, C.; Lucini, L.; Dall'Asta, M.; Ferrante, M.; Puglisi, E. The impact of metallic nanoparticles on gut fermentation processes: An integrated metabolomics and metagenomics approach following an in vitro digestion and fecal fermentation model. *J. Hazard. Mater.* **2023**, *453*, 131331−131339.
(31) Bai, T.; Lu, P.; Guo, Z.; Xiang, L.; Liu, L. A simple approach towards citrate-stabilized Ag nanoparticles with widely tunable sizes. *Colloids and Surfaces A: Physicochemical and Engineering Aspects.* **2018**, *540*, 143−149.
(32) Brodkorb, A.; Egger, L.; Alminger, M.; Alvito, P.; Assunção, R.; Ballance, S.; Bohn, T.; Bourlieu-Lacanal, C.; Boutrou, R.; Carrière, F.; Clemente, A.; Corredig, M.; Dupont, D.; Dufour, C.; Edwards, C.; Golding, M.; Karakaya, S.; Kirkhus, B.; Le Feunteun, S.; Lesmes, U.; Macierzanka, A.; Mackie, A. R.; Martins, C.; Marze, S.; McClements, D. J.; Ménard, O.; Minekus, M.; Portmann, R.; Santos, C. N.; Souchon, I.; Singh, R. P.; Vegarud, G. E.; Wickham, M. S. J.; Weitschies, W.; Recio, I. INFOGEST static in vitro simulation of gastrointestinal food digestion. *Nat. Protoc.* **2019**, *14*, 991−1014.
(33) Syafiuddin, A.; Salmiati, S.; Hadibarata, T.; Kueh, A. B. H.; Salim, M. R.; Zaini, M. A. A. Silver nanoparticles in the water environment in Malaysia: inspection, characterization, removal, modeling, and future perspective. *Sci. Rep.* **2018**, *8*, 986−994.
(34) Sahu, S. C. Altered global gene expression profiles in human gastrointestinal epithelial Caco2 cells exposed to nanosilver. *Toxicology Reports.* **2016**, *3*, 262−268.
(35) Pratsinis, A.; Hervella, P.; Leroux, J. C.; Pratsinis, S. E.; Sotiriou, G. A. Toxicity of silver nanoparticles in macrophages. *Small.* **2013**, *9*, 2576−2584.
(36) Tsugawa, H.; Cajka, T.; Kind, T.; Ma, Y.; Higgins, B.; Ikeda, K.; Kanazawa, M.; VanderGheynst, J.; Fiehn, O.; Arita, M. MS-DIAL: data-independent MS/MS deconvolution for comprehensive metabolome analysis. *Nature methods.* **2015**, *12*, 523−526.
(37) Axson, J. L.; Stark, D. I.; Bondy, A. L.; Capracotta, S. S.; Maynard, A. D.; Philbert, M. A.; Bergin, I. L.; Ault, A. P. Rapid kinetics of size and pH-dependent dissolution and aggregation of silver nanoparticles in simulated gastric fluid. *J. Phys. Chem. C* **2015**, *119*, 20632−20641.
(38) Ault, A. P.; Stark, D. I.; Axson, J. L.; Keeney, J. N.; Maynard, A. D.; Bergin, I. L.; Philbert, M. A. Protein corona-induced modification of silver nanoparticle aggregation in simulated gastric fluid. *Environmental Science: Nano.* **2016**, *3*, 1510−1520.
(39) Molleman, B.; Hiemstra, T. Time, pH, and size dependency of silver nanoparticle dissolution: the road to equilibrium. *Environmental Science: Nano.* **2017**, *4*, 1314−1327.
(40) Qin, D.; Yang, G.; Wang, Y.; Zhou, Y.; Zhang, L. Green synthesis of biocompatible trypsin-conjugated Ag nanocomposite with antibacterial activity. *Appl. Surf. Sci.* **2019**, *469*, 528−536.
(41) Li, X.; Wang, K.; Peng, Y. Exploring the interaction of silver nanoparticles with pepsin and its adsorption isotherms and kinetics. *Chemico-biological interactions.* **2018**, *286*, 52−59.
(42) Ernest, V.; Shiny, P.; Mukherjee, A.; Chandrasekaran, N. Silver nanoparticles: a potential nanocatalyst for the rapid degradation of starch hydrolysis by α-amylase. *Carbohydr. Res.* **2012**, *352*, 60−64.
(43) Sharma, N.; Parhizkar, M.; Cong, W.; Mateti, S.; Kirkland, M.; Puri, M.; Sutti, A. Metal ion type significantly affects the morphology but not the activity of lipase−metal−phosphate nanoflowers. *RSC advances.* **2017**, *7*, 25437−25443.
(44) Darvishi-Ganji, K.; Mirzajani, F.; Aliahmadi, A.; Fakhari-Zavareh, A.; Ghassempour, A. Silver nanoparticle trypsin corona formation and the impacts on enzymatic potency. *Phys. Chem. Res.* **2020**, *8*, 241−250.
(45) Fernando, I.; Zhou, Y. Concentration dependent effect of humic acid on the transformations of silver nanoparticles. *J. Mol. Liq.* **2019**, *284*, 291−299.
(46) Fernando, I.; Zhou, Y. Impact of pH on the stability, dissolution and aggregation kinetics of silver nanoparticles. *Chemosphere.* **2019**, *216*, 297−305.
(47) Xu, M.; Yang, Q.; Xu, L.; Rao, Z.; Cao, D.; Gao, M.; Liu, S. Protein target identification and toxicological mechanism investigation of silver nanoparticles-induced hepatotoxicity by integrating proteomic and metallomic strategies. *Part. Fibre Toxicol.* **2019**, *16*, 46−53.
(48) Butler, K. S.; Peeler, D. J.; Casey, B. J.; Dair, B. J.; Elespuru, R. K. Silver nanoparticles: correlating nanoparticle size and cellular uptake with genotoxicity. *Mutagenesis.* **2015**, *30*, 577−591.

(49) Gliga, A. R.; Skoglund, S.; Wallinder, I. O.; Fadeel, B.; Karlsson, H. L. Size-dependent cytotoxicity of silver nanoparticles in human lung cells: the role of cellular uptake, agglomeration and Ag release. *Part. Fibre Toxicol.* **2014**, *11*, 1−17.
(50) Barbalinardo, M.; Caicci, F.; Cavallini, M.; Gentili, D. Protein corona mediated uptake and cytotoxicity of silver nanoparticles in mouse embryonic fibroblast. *Small* **2018**, *14*, 1−12.
(51) Jiang, X.; Wu, Y.; Gray, P.; Zheng, J.; Cao, G.; Zhang, H.; Zhang, X.; Boudreau, M.; Croley, T. R.; Chen, C.; Yin, J. J. Influence of gastrointestinal environment on free radical generation of silver nanoparticles and implications for their cytotoxicity. *NanoImpact* **2018**, *10*, 144−152.
(52) McCracken, C.; Zane, A.; Knight, D. A.; Hommel, E.; Dutta, P. K.; Waldman, W. J. Oxidative stress-mediated inhibition of intestinal epithelial cell proliferation by silver nanoparticles. *Toxicology In Vitro.* **2015**, *29*, 1793−1808.
(53) Araki, Y.; Katoh, T.; Ogawa, A.; Bamba, S.; Andoh, A.; Koyama, S.; Fujiyama, Y.; Bamba, T. Bile acid modulates transepithelial permeability via the generation of reactive oxygen species in the Caco-2 cell line. *Free radical biology and medicine.* **2005**, *39*, 769−780.
(54) Bibi, S.; Huguet-Tapia, J. C.; Afzal, N. Z.; El-Sayed, A. S. A. F.; Timilsina, S.; Jones, J. B.; Ali, G. S. Study of silver nanoparticle effects on some molecular responses and metabolic pathways of Phytophthora parasitica. *Int. J. Nanomater. Nanotechnol. Nanomed.* **2021**, *7*, 047−056.
(55) Tang, D.; Chen, X.; Kang, R.; Kroemer, G. Ferroptosis: molecular mechanisms and health implications. *Cell research.* **2021**, *31*, 107−125.
(56) Singh, N.; Barnych, B.; Wagner, K. M.; Wan, D.; Morisseau, C.; Hammock, B. D. Adrenic acid-derived epoxy fatty acids are naturally occurring lipids and their methyl ester prodrug reduces endoplasmic reticulum stress and inflammatory pain. *ACS omega.* **2021**, *6*, 7165−7174.
(57) Babcock, T.; Helton, W.; Espat, N. J. Eicosapentaenoic acid (EPA): an antiinflammatory ω-3 fat with potential clinical applications. *Nutrition.* **2000**, *16*, 1116−1118.
(58) Kagan, V. E.; Mao, G.; Qu, F.; Angeli, J. P. F.; Doll, S.; St Croix, C.; Dar, H.; Liu, B.; Tyurin, V. A.; Ritov, V. B. Oxidized Arachidonic/Adrenic Phosphatidylethanolamines Navigate Cells to Ferroptosis. *Nat. Chem. Biol.* **2016**, *19*, 2238−2246.
(59) Dixon, S. J.; Lemberg, K. M.; Lamprecht, M. R.; Skouta, R.; Zaitsev, E. M.; Gleason, C. E.; Patel, D. N.; Bauer, A. J.; Cantley, A. M.; Yang, W. S.; Morrison, B.; Stockwell, B. R. Ferroptosis: an iron-dependent form of nonapoptotic cell death. *Cell* **2012**, *149*, 1060−1072.
(60) Hadian, K. Ferroptosis suppressor protein 1 (FSP1) and coenzyme Q10 cooperatively suppress ferroptosis. *Biochemistry.* **2020**, *59*, 637−638.
(61) Deshwal, S.; Onishi, M.; Tatsuta, T.; Bartsch, T.; Cors, E.; Ried, K.; Lemke, K.; Nolte, H.; Giavalisco, P.; Langer, T. Mitochondria regulate intracellular coenzyme Q transport and ferroptotic resistance via STARD7. *Nat. Cell Biol.* **2023**, *25*, 246−257.
(62) Pérez, R.; Matabosch, X.; Llebaria, A.; Balboa, M. A.; Balsinde, J. Blockade of arachidonic acid incorporation into phospholipids induces apoptosis in U937 promonocytic cells. *Journal of lipid research.* **2006**, *47*, 484−491.
(63) Kuwata, H.; Hara, S. Role of acyl-CoA synthetase ACSL4 in arachidonic acid metabolism. *Prostaglandins Other Lipid Mediators* **2019**, *144*, 1−9.
(64) Hoshyar, N.; Gray, S.; Han, H.; Bao, G. The effect of nanoparticle size on in vivo pharmacokinetics and cellular interaction. *Nanomedicine.* **2016**, *11*, 673−692.
(65) Zhang, S.; Li, J.; Lykotrafitis, G.; Bao, G.; Suresh, S. Size-dependent endocytosis of nanoparticles. *Advanced materials (Deerfield Beach, Fla.).* **2009**, *21*, 419−426.
(66) Liu, X.; Huang, N.; Li, H.; Jin, Q.; Ji, J. Surface and size effects on cell interaction of gold nanoparticles with both phagocytic and nonphagocytic cells. *Langmuir.* **2013**, *29*, 9138−9148.
(67) Huang, J.; Bu, L.; Xie, J.; Chen, K.; Cheng, Z.; Li, X.; Chen, X. Effects of nanoparticle size on cellular uptake and liver MRI with polyvinylpyrrolidone-coated iron oxide nanoparticles. *ACS Nano* **2010**, *4*, 7151−7160.

https://doi.org/10.1021/acsnanoscienceau.4c00012
ACS Nanosci. Au 2024, 4, 327−337